Trapped magnetic flux in superconducting niobium samples

S. Aull, O. Kugeler, and J. Knobloch

Helmholtz-Zentrum, Berlin, Germany

Trapped magnetic flux is known to be one cause of residual losses in bulk niobium superconducting radio frequency cavities. In the Meissner state an ambient magnetic field should be expelled from the material. Disturbances such as lattice defects or impurities have the ability to inhibit the expulsion of an external field during the superconducting transition so that the field is trapped. We have investigated the effect the treatment history of bulk niobium has on the trapped flux and which treatment leads to minimal flux trapping. For that purpose, we measured the fraction of trapped magnetic flux in niobium samples representing cavities with different typical treatment histories. The differences between single crystal and polycrystalline material as well as the influence of spatial temperature gradients and different cooling rates were investigated. In addition, the progression of the release of a trapped field during warm-up was studied. We found that heat treatment reduces trapped flux considerably and that single crystal samples trap less flux than polycrystalline niobium. As a consequence, the single crystal sample with 1200°C baking trapped the smallest amount of field which is about 42%. Moreover, the release of the trapped field during warm-up was observed to progress over a broad temperature range for the baked single crystal samples.

I. INTRODUCTION

The surface resistance defines the dissipated power in a superconducting radio frequency (SRF) cavity. It consists basically of two contributions. The BCS contribution described by the BCS theory decreases exponentially with temperature and increases with the square of the operating frequency. In addition to the BCS contribution there is a residual resistance which is temperature independent. At a typical operating temperature of 2 K, the residual resistance often accounts for more than 30% of the total surface resistance [1].

SRF cavities are operated in the Meissner state so an external magnetic field should be expelled from the material, see Fig. 1(a). Imperfections of the crystal lattice like impurities, dislocations, and grain boundaries have the ability to suppress the expulsion of magnetic field during the superconducting transition. The field remains in the material even after switching off the source of the external magnetic field, see Fig. 1(b). This trapped field penetrates the material in the form of flux tubes which have a normal conducting core. The unpaired electrons in these normal conducting areas cause an Ohmic resistance and therefore contribute to the residual surface resistance.

The residual resistance increases linearly with the trapped field and depends on the operating frequency:

*sarah.aull@helmholtz-berlin.de

$$R_{\text{res}} = \alpha H_{\text{trap}} \sqrt{f/\text{GHz}}, \qquad (1)$$

where α describes the sensitivity of the surface resistance on the trapped field. It has to be determined experimentally, e.g., Ref. [2] found $\alpha = 2.2 \frac{\text{n}\Omega}{\mu\text{T}}$ for a bulk niobium, 1.5 GHz single cell cavity.

At 1.3 GHz, the additional surface resistance due to trapped flux would be 125 nΩ if no magnetic shielding is provided and the earth magnetic field of about 50 μT is trapped completely. In terms of the quality factor Q_0 this would mean that, for example, a cavity with a fairly high quality factor of 10^{10} would be downgraded to 2×10^9 which implies the need for a 5 times larger cryoplant.

In the early 1990's, Vallet *et al.* already measured 100% flux trapping when exposing niobium to external fields up to 300 μT [3]. At 2 K and 1.3 GHz, the surface resistance typically is 15 nΩ [4]. If a magnetic shield with 95% efficiency is used, then the earth's field would account for nearly half of this residual resistance (6.3 nΩ). Since a cryoplant has a very poor efficiency (in the order of 1:1000) minimizing the surface resistance and therefore the losses means reducing operation and installation costs significantly, especially for cw machines.

The flux trapping mechanisms have predominantly been studied in the Shubnikov phase of type II superconductors which is energetically favorable when an ambient magnetic field penetrates the material. In the Shubnikov phase, the magnetic field forms a hexagonal lattice of quantized flux tubes. A lot of calculations were done, estimating the interaction between the flux tube lattice and the variation in the lattice defects distribution. Pinning forces of different

(a) Sketch of the perfect Meissner effect
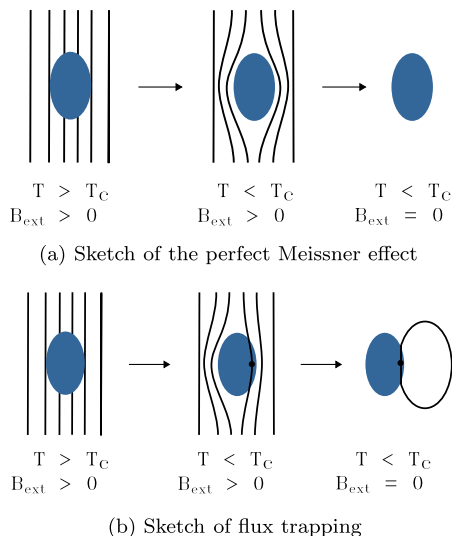

(b) Sketch of flux trapping

FIG. 1.   Comparison between the perfect Meissner effect and the suppression of the flux expulsion due to flux pinning.

kinds of pinning centers, the interaction among the flux tubes themselves as well as the coexistence of normal conducting and superconducting areas (*intermediate state*) are subjects of recent studies. An overview of these topics can be found in Ref. [5].

Nevertheless, it remains doubtful whether these findings are applicable to trapped flux in the Meissner phase as the penetration of the magnetic flux is neither energetically favorable nor organized in a hexagonal lattice.

The goal of the experiments reported here was to study the flux trapping in representative niobium samples to better understand the impact of treatment history and operating conditions on flux trapping. All measurements were performed in the Meissner state.

Apart from that, past measurements suggest that thermal gradients will generate currents by the Seebeck effect [6]. We tested if these thermal currents generate additional magnetic fields. If additional fields in the order of μT are generated and trapped, this effect has to be accounted for cavity operation since an additional residual surface resistance of several nΩ would be caused.

II. EXPERIMENT

A. Setup

We constructed a scanning device capable of generating flux in niobium disks and scanning the field with the niobium in the superconducting state. The setup was installed in the HoBiCaT facility at the Helmholtz-Zentrum Berlin [7].

Figure 2 shows the top view of the sample holder made from copper which is connected to the cooling table of the cryostat. It provides four sample positions and is cooled to 6 K. The niobium samples are located under rectangular copper covers.
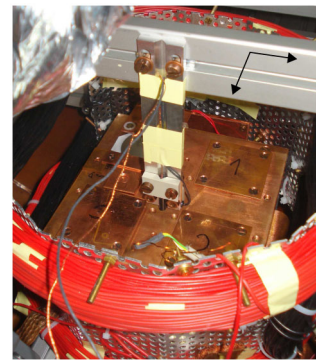

FIG. 2.   Setup to scan trapped flux in Nb samples.

Because of a thermal short circuit, the niobium samples warm up uniformly. This was verified by temperature sensors. At the center of each sample position is a bore hole through which a Cernox$^{\text{TM}}$ temperature sensor can be attached to the sample.

Two heater foils serve as heat sources in order to quickly cycle the samples between normal and superconducting state without warming up the whole cryostat. By varying the heater's power output, an equilibrium temperature as well as heating rate and cooling rate could be defined.

The magnetic field measurements were done with the fluxgate magnetometer *Mag-01H* from Bartington Instruments®. This single axis probe is suitable for low field measurements and cryogenic applications. The technical data sheet claims a measurement range from 0 to 290 μT with a resolution of 1 nT in the range of 0–100 μT and 10 nT in the range of 100–290 μT. The probe has a cylindrical shape with a length of 32 mm and a diameter of 6 mm. It can be moved into the two lateral directions which enables measurements of four samples and scanning the field over each sample.

Two pairs of coils were installed in order to generate external magnetic fields perpendicular (Helmholtz coils) as well as parallel (racetrack coils) to the sample surface. Using the racetrack coils, external fields up to $B_y = 200$ μT were produced. The Helmholtz coils were placed above and below the sample holder and generated up to $B_z = 2.3$ mT. The produced magnetic field varies over the sample area less than 2%.

A detailed description and characterization of the measurement device can be found in Ref. [8].

B. Samples

A list of all measured samples can be found in Table I. The niobium samples differ in crystal structure and in their treatment history. Tempering at different temperatures dissolves hydrogen (800°C) and light elements (1200°C) and homogenizes the material.

The *buffered chemical polishing* (BCP) removes the surface layer which is damaged during the fabrication

TABLE I. List of measured samples—all samples had a residual resistance ratio of about 260 before the treatment.

Sample	Crystal structure	Treatment
1	Polycrystalline	None
2	Polycrystalline	BCP
3	Polycrystalline	BCP + 800°C
4	Single crystal	BCP
5	Single crystal	BCP + 800°C
6	Single crystal	BCP + 1200°C

process. 140–160 μm were removed from each treated sample. In case of tempered samples an additional short BCP (about 14 μm removal) was done after tempering.

The samples are disks of 37–48 mm diameter and have 2.6–3.1 mm thickness.

Comparing the samples with each other allows drawing conclusions about the effect of grain boundaries, interstitial gases and dislocations, and the condition of the surface on trapped magnetic flux.

C. Measurement procedure

A magnetic field was trapped in the sample the following way: (i) the sample is warmed up to the normal conducting state ($T > T_c$); (ii) the Helmholtz coils are switched on, applying a magnetic field $B_{applied}$; (iii) the sample is cooled to the superconducting state ($T < T_c$); (iv) the Helmholtz coils are switched off; (v) the field probe measures any remaining field which is considered to be the trapped magnetic field $B_{trapped}$.

The residual magnetic field due to imperfect shielding is 1–3.5 μT. It is noted for every probe position and deducted from the measurement values. As the field probe measures the magnetic field at a certain distance above the sample, the field on the sample surface has to be calculated. This is outlined in the following section.

D. Field simulation

The 32 mm long magnetic field probe measures the field in its center as indicated in Fig. 3. Therefore, all measured data has to be corrected to the surface of the sample.

For that purpose, the magnetic field of a magnetized disk was simulated. The software package RADIA was used to
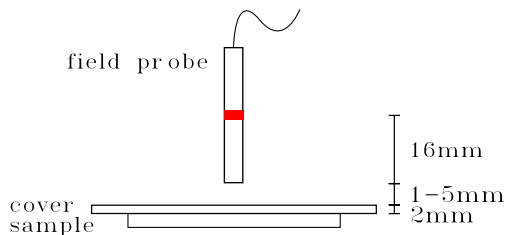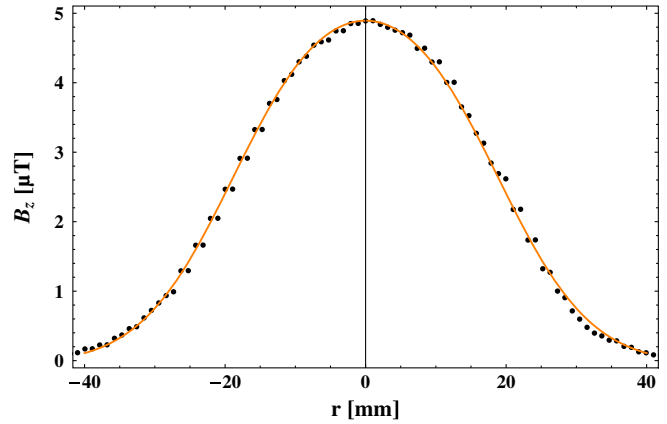
FIG. 3. Position of the field probe above the sample.

FIG. 4. Calculated magnetic field of a homogeneously magnetized disk at the probe position compared to the measured trapped field as a function of the radius.

define an object with the sample geometry and to allot a homogeneous magnetization in the direction of interest. The magnetic field was then calculated at a certain distance above the disk's surface which corresponds to the distance between the field probe and the sample surface.

Additionally, the magnetic field was calculated at a fixed height as a function of the radius. For comparison, the profile of the trapped field was measured in the lateral direction.

Figure 4 compares the calculated magnetic field at the probe position as a function of the radial position with the measured magnetic field. The comparison of the measured lateral profile with the simulated one confirms that the assumption of a uniformly magnetized disk within the resolution of the sensor is reasonable. Thus, the field at the surface is related to the measured field at the probe position by a constant factor which we used to quantify the percentage of trapped flux.

III. RESULTS

A. Influence of treatment and field strength

All samples were exposed to ambient fields up to 300 μT. Additionally, ambient fields up to 2.3 mT were applied to the untempered polycrystalline samples (samples 1 and 2). The fluxgate magnetometer was positioned above the center of the sample, i.e., at the maximum of trapped field profile. The amount of the trapped field as function of the applied field can be found in Fig. 5.

It was observed that each sample traps a fixed fraction of the applied field independent of the strength of the applied field. This implies that the flux lines do not interact with each other.

The fraction of the trapped field on the surface was calculated from the measured data. The total fraction of trapped field for each sample can be found in Table II.

TABLE II. Flux trapping behavior of all measured samples. Only single crystal samples showed a dependence on the cooling rate v (in mK/s). All measurements were done for $1 < v < 80$ mK/s.

Sample	Crystal structure	Treatment	Fraction of trapped flux
1	Polycrystalline	None	100%
2	Polycrystalline	BCP	100%
3	Polycrystalline	BCP + 800°C	$(83.1 \pm 0.8)\%$
4	Single crystal	BCP	$[(72.9 + 0.1\ln v) \pm 0.8]\%$
5	Single crystal	BCP + 800°C	$[(61.6 + 1.3\ln v) \pm 0.8]\%$
6	Single crystal	BCP + 1200°C	$[(42.1 + 0.13\ln v) \pm 0.6]\%$

The fraction is greatest for untempered polycrystalline samples (100%) and least for heat-treated single crystal samples (ca. 40%).

Sample 6 is a single crystal sample with BCP treatment which was baked at 1200°C. So, there are no grain boundaries and presumably less hydrogen, interstitials, and dislocations in the bulk. It can be speculated that the remaining 40% trapped flux then are due to the natural
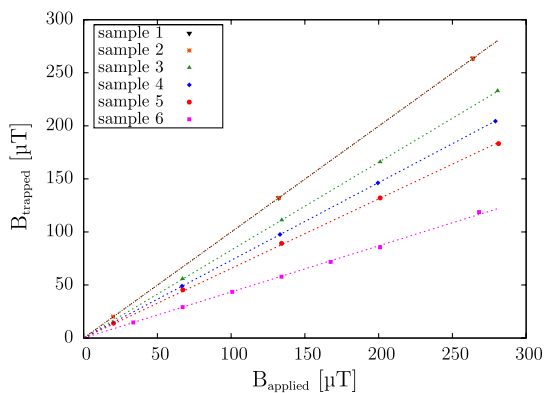

FIG. 5. Dependency of the trapped field on the applied field for all measured samples: None of the samples exhibited a dependency on the applied field. The data for samples 1 and 2 overlap—they both trap 100% of the applied field.
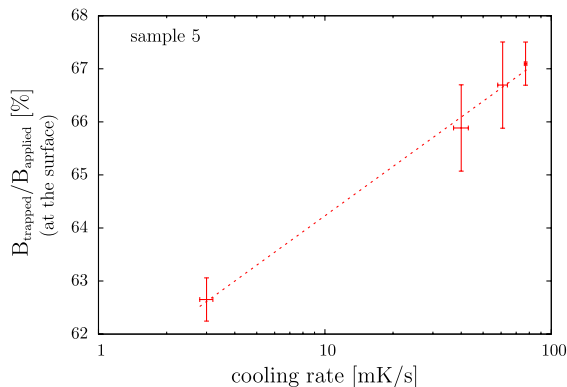

FIG. 6. Dependence of the trapped field on the cooling rate for a single crystal sample with 800°C tempering.

oxide surface layer of the niobium sample. The influence of the oxide layer will be studied in the future.

B. Influence of the cooling rate

The fraction of trapped magnetic field was also measured as a function of the cooling rate v. Cooling rates in the range of 0.5–60 mK/s could be produced.

A logarithmic dependence on the cooling rate was found for all single crystal samples within the measurement range. Polycrystalline samples showed no dependence, i.e., they trap 100%, respectively 83.1%, regardless of the cooling rate. Figure 6 shows the fraction of trapped field as a function of the cooling rate for the 800°C tempered single crystal sample. It seems likely that this effect is suppressed in the polycrystalline samples since grain boundaries seem to have the strongest pinning force so that all flux flow is prevented.

C. Flux release

Additionally, the transition from the superconducting to the normal conducting state and the associated release of trapped flux was examined. For that purpose, a sample with a trapped field was warmed up very slowly until the trapped field vanished.
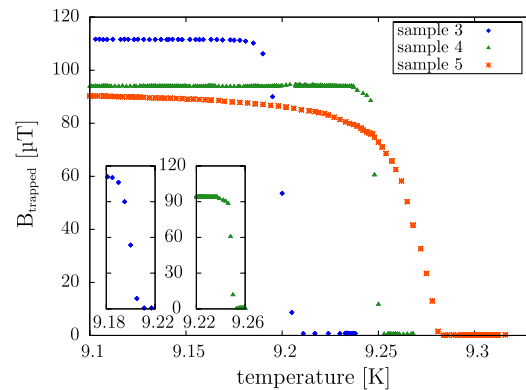

FIG. 7. Release of the trapped field during warm-up: The tempered single crystal samples released the trapped field over a broad temperature range.
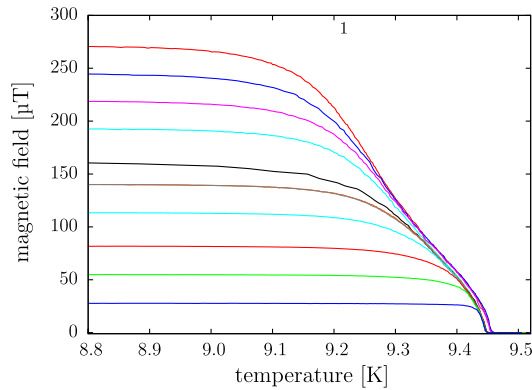
FIG. 8.   Release of different trapped fields during warm-up for a single crystal sample with 1200°C tempering.

FIG. 10.   Progression of the temperature gradient and the magnetic field due to the Seebeck effect superimposed with the heater fields for both current directions. The heater was switched on at $t = 120$ s to establish a temperature gradient. It was switched off at $t = 1120$ s.

Figure 7 shows the release of a trapped field for the samples 3, 4, and 5. It was observed that the tempered single crystal samples (no. 5 and no. 6) release the trapped fields within a broad temperature range. For all other samples the transition was significantly less broad. The narrowest transition is observed with polycrystalline niobium.

Figure 8 shows the progression of the flux release for different trapped fields. It can be seen that the higher the trapped field is the lower is the temperature where the release starts. Nevertheless, the progression near T_c is the same. This implies that in the temperature range just below T_c, the absolute amount of field that can be trapped depends on the temperature.

We found that during the flux release the sample was still fully in the superconducting state by the following test: During the release the heater was turned off so that the samples cooled down again. Simultaneously, the Helmholtz coils were switched on again. After reaching the cool equilibrium temperature, the level of trapped field was measured.

It was found that the amount of trapped field remained unchanged at the level when the heating was aborted. No additional flux was trapped due to the applied field and it can be concluded that the sample was therefore completely superconducting so that no new flux could enter.

D. Thermal currents

One of the sample positions was designed in such a way that it allowed the generation of a spatial temperature gradient of about 0.5 K/cm over the sample. This is illustrated in Fig. 9.

The sample is placed on a piece of polytetrafluoroethylene (PTFE) to inhibit the cooling from below. At one side
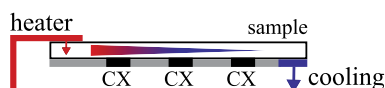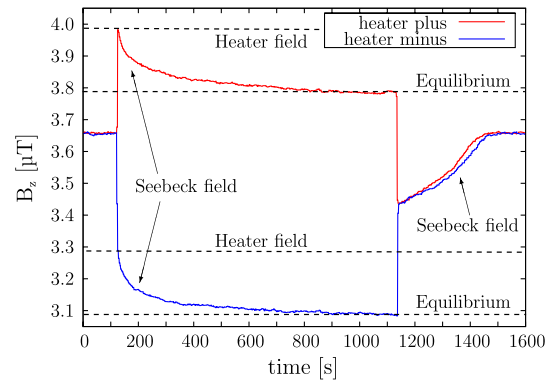

FIG. 9.   Sketch of the generation of a temperature gradient over one sample.

of the sample a heater was attached while at the opposite side the sample was connected to the sample holder to provide cooling. The temperature was measured at three points on the bottom side of the sample.

Because of the thermoelectric effect (Seebeck effect), a temperature gradient produces a thermal current and therefore an additional magnetic field (*Seebeck field*). We were able to confirm the existence of such a field at cryogenic temperatures when the sample was above T_c.

Unfortunately, the measured strength of the Seebeck field was of the same order as the field generated by the heater current used to establish the thermal gradient. To separate out the effect, the experiment was repeated twice with opposite polarity of the heater current, but the same power. The difference of the magnetic field measurement then yields the Seebeck field since the magnetic field due to thermal currents does not change the orientation when the heater current is reversed.

Figure 10 depicts the measured magnetic field which is a superposition of the constant field produced by the heater and the field induced by the thermal current as long as the heater is switched on. After switching on the heater a negatively oriented field builds up due to the rising temperature gradient, superposing the constant heater field. After switching off the heater ($t > 1120$ s), there is no heater field and the decrease of the pure Seebeck field can be observed.

Additionally, the temperature gradient is shown (right scale) as a function of time. The progression of the gradient after switching off the heater seems unexpected. The one temperature sensor is close to the cooling side while the other one is close to the heater side where the sample is isolated by PTFE. It can be assumed that the cooling proceeds slower on the heater side (due to the isolation) so that the temperature gradient gets bigger at first. After a certain time elapsed, the isolated side is cooled too and the temperature gradient vanishes.

S. AULL, O. KUGELER, AND J. KNOBLOCH

Phys. Rev. ST Accel. Beams **15,** 062001 (2012)

IV. CONCLUSION

The measurements showed that the treatment history of the niobium samples has a great influence on the trapping behavior. The *fraction* of trapped flux seems to depend on the impurity content and strongly on the number of grain boundaries. Especially the results of the tempered samples support previous experiments (compare Refs. [9,10]). By contrast, no influence of the strength of the applied field was found which implies that there is no flux line interaction. In addition no influence of the BCP treatment was observed for the polycrystalline samples.

Additionally, the release of the trapped field over a broad temperature range was observed for the tempered single crystal samples although the samples were shown to be superconducting during the flux release near T_c. As the progression of the flux release is the same, independently from the amount of trapped field in the cold equilibrium, one could guess that the absolute value of field that can be trapped depends on the temperature as long as the sample temperature is about tens of mK below T_c.

The tempered single crystal samples exhibited the least amount of flux trapping and, hence, must have weaker pinning centers. One speculation is that, as T_c is approached, the thermal energy of the flux tubes suffices for depinning, leading to gradual flux release. This will be the subject of future measurements. In general, it seems likely that the release of trapped flux just below T_c is due to temperature and field dependence of the pinning mechanism.

Moreover, it could be shown that a local temperature gradient induces an additional magnetic field. Even a small temperature gradient induces magnetic fields that are of the same order as the residual magnetic fields in a cryostat due to imperfect shielding (about 1 μT). Therefore, thermal currents during cooldown may affect the performance of SRF cavities.

[1] P. Schmüser, in *CERN Accelerator School Intermediate Accelerator Physics* (CERN, Geneva, 2003), pp. 183–202.

[2] P. Kneisel and B. Lewis, Contunuous Electron Bean Accelerator Facility Technical Report No. 94-028, 1994.

[3] C. Vallet, M. Bolor, B. Bonin, J. P. Charrier, B. Daillant, J. Gratadour, F. Koechlin, and H. Safa, in Proceedings of the 3rd European Particle Accelerator Conference, Berlin, Germany (1992), pp. 1295–1297.

[4] B. Aune, R. Bandelmann, D. Bloess, B. Bonin, A. Bosotti, M. Champion, C. Crawford, G. Deppe, B. Dwersteg, D. Edwards, H. Edwards, M. Ferrario, M. Fouaidy, P.-D. Gall, A. Gamp, A. Gössel, J. Graber, D. Hubert, M. Hüning, M. Juillard, T. Junquera, H. Kaiser, G. Kreps, M. Kuchnir, R. Lange, M. Leenen, M. Liepe, L. Lilje, A. Matheisen, W.-D. Möller, A. Mosnier, H. Padamsee, C. Pagani, M. Pekeler, H.-B. Peters, O. Peters, D. Proch, K. Rehlich, D. Reschke, H. Safa, T. Schilcher, P. Schmüser, J. Sekutowicz, S. Simrock, W. Singer, M. Tigner, D. Trines, K. Twarowski, G. Weichert, J. Weisend, J. Wojtkiewicz, S. Wolff, and K. Zapfe, Phys. Rev. ST Accel. Beams **3**, 25 (2000).

[5] R. Huebener, *Magnetic Flux Structures in Superconductors*, edited by M. Cardona, P. Fulde, K. v. Klitzing, H.-J. Queisser, R. Merlin, and H. Störmer, Springer Series in Solid-State Science Vol. 6 (Springer, New York, 2001), 2nd ed., p. 311.

[6] J. Knobloch and H. Padamsee, in Proceedings of the 8th Workshop on RF Superconductivity, Padova, Italy (1997), pp. 337–344.

[7] O. Kugeler, A. Neumann, and W. Anders, and J. Knobloch, Rev. Sci. Instrum. **81**, 074701 (2010).

[8] S. Aull, Diplomarbeit, Humboldt-Universität Berlin, 2011.

[9] G. Ciovati and A. Gurevich, in Proceedings of the 13th Workshop on RF Superconductivity, Berlin, Germany (2007), pp. 132–136.

[10] C. Benvenuti, S. Calatroni, I. Campisi, P. Darriulat, C. Durand, M. Peck, R. Russo, and A.-M. Valente, in Proceedings of the 8th Workshop on RF Superconductivity, Padova, Italy (1997), pp. 331–335.